The following publication X. Luo, S. Xia, K. W. Chan and X. Lu, "A Hierarchical Scheme for Utilizing Plug-In Electric Vehicle Power to Hedge Against Wind-Induced Unit Ramp Cycling Operations," in IEEE Transactions on Power Systems, vol. 33, no. 1, pp. 55-69, Jan. 2018 is available at https://doi.org/10.1109/TPWRS.2017.2696540.

A Hierarchical Scheme for Utilizing Plug-in Electric Vehicle Power to Hedge against Wind-induced Unit Ramp Cycling Operations

Xiao Luo, S. W. Xia, *Member, IEEE*, K. W. Chan, *Member, IEEE*, X. Lu

***Abstract*—Increasing wind power (WP) integration is forcing conventional units to go through more frequent and significant cycling operations, which would accelerate wear and tear to unit components and eventually affect the unit's lifespan. In this context, this paper proposes a hierarchical scheme to control the power of plug-in electric vehicles (PEVs) to mitigate unit ramp cycling (URC) operations. A general-form representation of the URC operation is proposed for the first time. At the top level of the hierarchical scheme, a system net load variation range (NLVR) is constructed first to capture the uncertainty in WP forecasts, and then the PEV power is scheduled to reshape the NLVR so as to minimize the URC operations that can be caused by the possible net load realizations in the NLVR. Based on updated WP forecasts, the middle-level dispatch model exempts over-scheduled anti-URC regulation onus on PEVs to promote PEV charging. At the bottom-level, a decentralized PEV charging control strategy is used to implement the PEV power dispatch instruction. Simulation results verify that the proposed scheme can avert the URC operations effectively while preserve most of the desired PEV charging energy. Simulation results also show that the proposed scheme is more capable of withstanding WP forecast errors compared with its deterministic version and a benchmark scheme.**

***Index Terms*—Hierarchical scheme, unit ramp cycling operations, plug-in electric vehicles, wind power**

NOMENCLATURE

A. Sets

AI	Set of indexes for PEV aggregators.
A_k	Set of indexes for PEVs controlled by the k^{th} aggregator.
I	Set of indexes for generators.
T	Set of indexes for timeslots.

B. Variables

ds_{t+nd}	Directing signal in the bottom-level decentralized PEV charging control strategy in sub-slot *nd* of timeslot *t*.
e	Index of PEV.
$g_{i,t}$	Power output of generator *i* in timeslot *t*.
$\overline{g}_{i,t}$	Power output of unit *i* in timeslot *t* corresponding to the upper bound of the NLVR.
$\underline{g}_{i,t}$	Power output of unit *i* in timeslot *t* corresponding to the lower bound of the NLVR.
i	Index of generator.
p_t^{PEV}	System-level PEV power in timeslot *t*.
$r_{e,t+nd}$	Power of PEV *e* in sub-slot *nd* of timeslot *t*.
$rc_{i,t}$	Binary indicator for the URC operation of unit *i* in timeslot *t*.
$rc_{i,t}^{\text{up}}$	Binary indicator for the upward URC operation of unit *i* in timeslot *t*.
$rc_{i,t}^{\text{down}}$	Binary indicator for the downward URC operation of unit *i* in timeslot *t*.
$SOC_{e,t}$	Battery state-of-charge of PEV *e* in timeslot *t*, as a percentage of the battery capacity.
t	Index of timeslot.
t_c	Current timeslot.
$\mu_{e,t}$	Urgency level of charging of PEV *e* in timeslot *t*.

C. Parameters

a_i, b_i, c_i	Coefficients of the quadratic fuel cost function of unit *i*.
d	Width of sub-timeslot.
C_e^{batt}	Battery capacity of PEV *e*.
DT_e	Planned departure time of PEV *e*.
DI_t^{PEV}	PEV dispatch instruction in timeslot *t*.
$E_t^{\text{PEV\_ch}}$	Maximum amount of energy that can be charged to PEVs from the 1st to the t^{th} timeslot of the scheduling horizon.
$E_t^{\text{PEV\_dch}}$	Maximum amount of energy that can be discharged from PEVs from the 1st to the t^{th} timeslot of the scheduling horizon.
$\overline{G}_i$	Maximum power output of unit *i*.
$\underline{G}_i$	Minimum power output of unit *i*.
G_{i,t_c}^{disp}	Middle-level dispatch result of the power output of unit *i* in timeslot t_c.
$\overline{G}_{i,t}^{\text{sched}}$	Top-level scheduling result of the power output of unit *i* in timeslot *t* corresponding to the upper bound of the NLVR.
$\underline{G}_{i,t}^{\text{sched}}$	Top-level scheduling result of the power output of unit *i* in timeslot *t* corresponding to the lower bound of the NLVR.
LN	A large constant.
L_t	Non-PEV load in timeslot *t*.
NUF	Number of future timeslots with updated wind power forecasts.
OH	Number of timeslots in the optimization horizon.

The authors gratefully acknowledge the support of the Hong Kong Polytechnic University under Project G-UA3Z, and the Hong Kong Polytechnic University Research Studentships awarded to Dr. Luo, Dr. Xia and Mr. Lu for their research study.

X. Luo, S. W. Xia, K. W. Chan and X. Lu are with the Department of Electrical Engineering, The Hong Kong Polytechnic University, Hung Hom, Hong Kong (e-mail: luo.xiao.peter@connect.polyu.hk; s.w.xia@ncepu.edu.cn; eekwchan@polyu.edu.hk; harry.lu@connect.polyu.hk).

$PIPO_{e,t}$	Binary indicator for plug-in/plug-out (1/0) status of PEV *e* in timeslot *t*.
$P_t^{\text{PEV\_ch}}$	Aggregate charging power capacity of all connected PEVs in timeslot *t*.
$P_t^{\text{PEV\_dch}}$	Aggregate discharging power capacity of all connected PEVs in timeslot *t*.
$P_{t_c}^{\text{PEV\_disp}}$	Middle-level dispatch result regarding the PEV power in timeslot t_c.
$P_t^{\text{PEV\_sched}}$	Top-level scheduling result regarding the PEV power in timeslot *t*.
R_e^{ch}	Rated charging power of PEV *e*'s battery.
R_e^{dch}	Rated discharging power of PEV *e*'s battery.
$R_{e,t_n}^{\text{unctl\_ch}}$	Uncontrolled charging power received by the battery of PEV *e* in timeslot t_n.
$R_{e,t_n}^{\text{max\_dch}}$	V2G power delivered from the battery of PEV *e* in timeslot t_n when it is plugged-in and discharging at maximum rate until the minimum allowable SOC is reached.
$RC_{i,t_c}^{\text{up\_disp}}$	Middle-level dispatch result regarding the upward URC operation of unit *i* in timeslot t_c.
$RC_{i,t_c}^{\text{down\_disp}}$	Middle-level dispatch result regarding the downward URC operation of unit *i* in timeslot t_c.
$RCTHR_i$	Threshold for the URC operation of unit *i*.
SW	Width of timeslot.
$SURL_i$	Start-up ramp rate limit of unit *i*.
$SDRL_i$	Shut-down ramp rate limit of unit *i*.
SOC_e^{desired}	Desired battery state-of-charge of PEV *e* upon its planned departure time.
$U_{i,t}$	Binary indicator for the on/off (1/0) status of unit *i* in timeslot *t*.
WS	Number of timeslots in the time window for identifying the URC operation.
$W_{t_c+n}^{\text{a}}$	Actual wind power in timeslot t_c+n.
$\overline{W}_t^{\text{UI}}$	Upper bound of the wind power uncertainty interval in timeslot *t*.
$\underline{W}_t^{\text{UI}}$	Lower bound of the wind power uncertainty interval in timeslot *t*.
$\overline{W}_{t_c+n}^{\text{UI\_upd}}$	Updated upper bound of the wind power uncertainty interval in t_c+n.
$\underline{W}_{t_c+n}^{\text{UI\_upd}}$	Updated lower bound of the wind power uncertainty interval in t_c+n.
β	Positive parameter affecting the pace of PEV power adjustment.
θ_{rc}	Coefficient for prioritizing the primary objective over the secondary objective.
θ_{fc}	Coefficient for prioritizing the secondary objective over the tertiary objective.
η_e	Charger efficiency of PEV *e*.
$\mu_e^{\max}$	Preset upper limit for the urgency level of charging of PEV *e*.

I. Introduction

POWER systems worldwide have been evolving towards a greener version by integrating more and more renewable energy sources, especially wind power (WP). On the one hand, higher penetration of wind energy would result in more and greater net load variations. On the other hand, the number of thermal units online will decrease as the system load is increasingly supplied by WP. Consequently, the thermal units will incur more frequent and significant cycling operations.

Unit cycling is defined as a generator being loaded at varying levels, including on/off cycling, ramp cycling (significant load following), and minimum load operations [1]. Generator components such as the boiler, gas pipes, and turbine will have to go through considerable thermal transient and pressure stress during cycling operations, which cause accelerated thermal fatigue, blade erosion and chemical deposit, among many other damaging mechanisms. Over time, the accumulated wear and tear to unit components will be translated into higher equivalent forced outage rates, higher maintenance and replacement costs, and ultimately shortened service life of the generator [1]–[3].

In [4]–[7], the damaging effect caused by unit on/off cycling operations was modeled by increasing the unit start-up cost or the operating cost in firing hours. These studies, however, did not consider the unit ramp cycling (URC) operation, which can be incurred at a much higher frequency than the on/off cycling operation in a system with considerable WP. The recognition of a URC operation should take into account both the magnitude and the duration of the generator power output change. In [3], the URC operation is defined as a change in an online generator's power output between two consecutive timeslots with magnitude greater than a preset threshold. This definition, however, does not cover the URC operations formed between two non-consecutive timeslots over a longer period of time. Other studies regarded a reverse of the direction of generator power output change (i.e. from increase to decrease, or vice versa) as an URC operation [8], [9]. This way of identifying the URC operation, however, has a distinct disadvantage that it fails to take into account the magnitude of the generator power output change, and thus can overstate the occurrence of the URC operation. To facilitate an adequate examination of the URC operation, a general-form representation of the URC operation is proposed in this paper.

In an effort to avert unit cycling operations induced by high-penetration WP, dynamic cycling costs was introduced in unit commitment (UC) in [3]. The results showed that the cycling burden was more evenly distributed among the generators. Yet, the majority of cycling operations (~63.6%) were still inevitable. Many other studies pointed out the need for deploying energy storage systems (ESSs) to better accommodate the WP uncertainty and variability. In [10], a battery-supercapacitor ESS was designed to realize controllable WP, where short-term rapid WP fluctuations were smoothed out by the supercapacitor while slow WP variations were compensated by the battery. The battery ESS (BESS) control schemes proposed in [11] and [12] aimed to limit the WP variance with the minimum battery capacity. This was achieved by using a first-order low-pass filter whose time constant was continuously optimized to determine the minimum battery power required for WP compensation. Similarly, another BESS control method proposed in [13] adopted a ramp rate limiter to identify the minimum required regulation power against photovoltaic and WP fluctuations.

With the growing popularity of plug-in electric vehicles

(PEVs) in many countries, PEV load is predicted to be an important part on the demand side of future smart grids. Since private car users usually park their cars for most of the time in a day and tend to follow routine schedules [14], most PEVs can remain grid-connected for a long period of time. This offers great controllability of the PEV load. Like ESSs, controllable PEVs have a great potential to provide large-scale buffering for WP. The aforementioned ESS control methods, however, may not be directly applicable to PEV power control. This is because while ESSs can be used exclusively for providing ancillary services for power systems as long as its stored energy is not depleted or saturated, the PEV power control needs to consider not only the provision of desired system regulation but also the fulfillment of PEV charging requirement.

Many studies in the literature have focused on controlling PEV power to mitigate the impact of WP intermittency on power system operations. In [15], how controlled PEV charging would affect the unit commitment and dispatch in the presence of large-scale WP was investigated. The results showed that the flexible PEV load can effectively reduce WP curtailment and limit the output variations of thermal units. In [16] and [17], PEVs were adopted to enhance the primary frequency regulation in a system with considerable renewable energy sources. However, PEVs participating in frequency regulation need to be charged and discharged frequently, and there will be an adverse impact on battery life. [18] suggested using the fast ramping capability of PEVs to enable the power system to accommodate higher level of renewable energy sources. A comprehensive model for introducing PEVs to the ramp market was proposed. When there is a large fast variation in net load, the PEV fleet will immediately deploy its fast ramping capacity to absorb the variation as much as possible while waiting for generators to catch up with their new generation points. After that, the PEVs will restore to their normal charging statuses. From the perspective of averting URC operations, the PEV power control methods proposed in [16]-[18] are barely effective because they only compensate for the scarcity of generator ramping capability, and the output variations of the renewable energy sources eventually need to be counterbalanced by the conventional units. [19] first scheduled PEV charging and WP generation to minimize the generator fuel cost, and then adopted a distributed charging control method to guide the PEV power in real time to counterbalance any deviations of the actual WP from the scheduled values. By so doing, the conventional units can adhere to their optimal generation schedules. The fuel cost minimization originates from flattened load curve; thus the likelihood of URC operations can also be reduced. However, depending on the differences between the actual and scheduled WP, the fulfillment of PEV charging demand can be compromised to various extents, and in [19] no measures were taken to handle this problem. In [20], the PEV power was controlled to regulate the actual load profile so as to let it follow a flattened load profile as close as possible. In this way the unexpected net load fluctuations due to WP intermittency will be neutralized by the PEV power adjustment rather than the output change of conventional generators. An important assumption made in [20] was that the average of net load forecast errors is approximately zero. Based on this assumption it was concluded that the fulfillment of PEV charging demand would only be slightly affected by the PEVs providing regulation services. However, historical data of actual and forecasted WP and load suggest that this assumption is questionable as it can be inconsistent with practical situations.

In this paper, a hierarchical scheme is proposed to schedule, dispatch, and control the PEV power to hedge against the URC operations in a system with considerable WP. The objective of this scheme is to minimize the URC operations while preserve as much PEV charging energy as possible. The scheme consists of 3 levels. At the top level, a variation range of the system net load is determined first to capture the WP uncertainty, and then, the PEV power is scheduled day-ahead to reshape the net load variation range (NLVR) to minimize the number of URC operations that can be caused by the possible net load realizations in the NLVR. Compared with the original NLVR, the reshaped NLVR will be much more resistant to WP variations with regard to avoiding the URC operation. Yet, the reshaped NLVR is usually at the cost of excessive interruptions to PEV charging, causing significant loss of the PEV charging energy. Based on the latest update of WP forecasts, the middle-level dispatch model will exempt over-scheduled anti-URC regulation onus on PEVs to promote PEV charging. However, due to the limited length of the dispatch horizon, the middle-level dispatch model may overly restore the PEV charging power, which will compromise the effectiveness of the PEV-aided URC operation mitigation. To avoid the over restoration, the reshaped NLVR from the top-level scheduling is used as an allowable range for the updated NLVR determined in the middle-level dispatch model. At the bottom level, a decentralized charging control strategy is used to guide the PEVs to implement the PEV power dispatch instruction from the middle-level model. The three-level structure of the proposed hierarchical scheme is visualized in Fig. 4.

The main contribution of this paper is twofold:

1) It proposes a general-form representation of the URC operation, which considers both the magnitude and the duration of the generator power ramp and incorporates a mechanism to prevent double-counting.
2) It proposes a hierarchical scheme for efficient utilization of PEV power to effectively hedge against URC operations.

The rest of the paper is organized as follows. In Section II, the construction of WP uncertainty intervals is introduced first; then the general-form representation of the URC operation is presented; finally, the proposed hierarchical scheme is formulated in detail. Section III presents a benchmark scheme. Section IV describes the simulation settings. The simulation results and analyses are presented in Section V. Conclusions are drawn in Section VI.

II. Formulation of The 3-Level Hierarchical Scheme

The proposed hierarchical scheme aims to minimize the

URC operation. Though the scheme can also be applied to reduce the on/off cycling operation, such application often causes prolonged and intense interruptions to PEV charging, which is likely to render the PEVs severely undercharged. Also, the PEV power which is scheduled to cooperate with UC could have reduced control flexibility for the proposed scheme to utilize for mitigating the URC operation. In this paper, it is assumed that a UC program without enabling PEV power control has been solved before the start of the proposed hierarchical scheme, and the generator on-off statuses in the hierarchical scheme are fixed to the UC solution.

A. Construction of the WP Uncertainty Interval

In the top-level scheduling model of the proposed scheme, the PEV power is coordinated to reshape the NLVR. The NLVR, which captures the uncertainty in WP forecasts, is obtained by superposing the WP uncertainty interval onto the system load profile. In each timeslot of the scheduling horizon, the WP uncertainty interval is a range of possible values for the actual WP in that slot. For a given WP forecast, the associated WP uncertainty interval can be derived from the corresponding historical data of the actual WP.

The procedures for constructing the WP uncertainty interval are given in [21] and recapped as follows. First, all WP data shall be normalized to per unit values based on the installed WP capacity. Second, the range of WP output from 0 to 1 p.u. is equally divided into K smaller intervals, where K is a user-defined integer. Each interval is referred to as a forecast grouping interval (FGI). For FGI k ($k = 1,2,\dots,K$), the actual WP data whose corresponding forecasts belong to FGI k will be collected. Thus, K datasets of actual WP can be obtained, in one-to-one correspondence with the K FGIs. Next, a probability histogram (PH) is constructed from each of the K actual WP datasets. The k^{th} PH represents the conditional probability distribution of the actual WP for a WP forecast belonging to FGI k. Then, a set of cumulative probabilities can be calculated from each PH to represent the corresponding cumulative distribution function (CDF).

In timeslot t, if the WP forecast belongs to FGI k and the WP uncertainty interval is required to cover Q% of the possible values for the actual WP suggested by the historical data, then the upper and lower bounds of the WP uncertainty interval are determined as follows:

$$\overline{W}_t^{\text{UI}} = F_k^{-1}((1+Q\%)/2) \tag{1}$$

$$\underline{W}_t^{\text{UI}} = F_k^{-1}((1-Q\%)/2) \tag{2}$$

where F_k^{-1} is the inverse CDF of the k^{th} actual WP dataset.

In a system with high WP penetration, WP uncertainty is often the dominant contributor to the net load uncertainty, as is the case with the WP and load data adopted in the simulation of this paper. As shown in Section IV, the load forecast errors are relatively less significant compared with the WP forecast errors. Thus, here the non-PEV load is assumed to be deterministic. Nevertheless, it shall be emphasized that the load uncertainty is still an important factor affecting the overall NLVR. The convolution of WP and load uncertainties can be captured by directly constructing the NLVR from net load historical data following the similar procedures for constructing the WP uncertainty interval.

B. Representation of the URC Operation

Whether a generator power output change is regarded as a URC operation depends on the magnitude and duration of the change. In this paper, a general-form representation of the URC operation is proposed as follows:

$$\begin{aligned} &|g_{i,t} - g_{i,t-1}| - LN \cdot rc_{i,t} \le RCTHR_i \\ &\quad + LN(2 - U_{i,t} - U_{i,t-1}), \forall i \in I, \forall t \in T \end{aligned} \tag{3}$$

$$\begin{aligned} &|g_{i,t} - g_{i,t-k}| - LN \cdot rc_{i,t} \le RCTHR_i + LN(k+1-\sum_{r=0}^{k} U_{i,t-r}) \\ &+ LN\sum_{h=1}^{k-1} rc_{i,t-h}, \forall i \in I, \forall t \in T, \forall k = 2 \dots WS-1 \end{aligned} \tag{4}$$

The inequalities (3) and (4) reflect that one URC operation can be developed between any two timeslots, consecutive or not, within the WS-slot time window. $rc_{i,t}$ will be set to 1 only if $\left|g_{i,t} - g_{i,t-m}\right| > RCTHR_i$, where m=1…WS-1. The second terms on the right-hand side of (3) and (4) are used to ensure that a URC operation is a power output change of an online generator so as to distinguish the URC operation from the on/off cycling operation. The third term on the right-hand side of (4) is used to avoid double-counting the URC operation. That is, the generator power output change between timeslot t and t-k, even if being greater than the ramp cycling threshold, should not be regarded as a URC operation if there has been a URC operation already formed in an intermediate timeslot t-h (t-k<t-h<t). Thus, the output changes which have accounted for one URC operation will not repeatedly contribute to the formation of another.

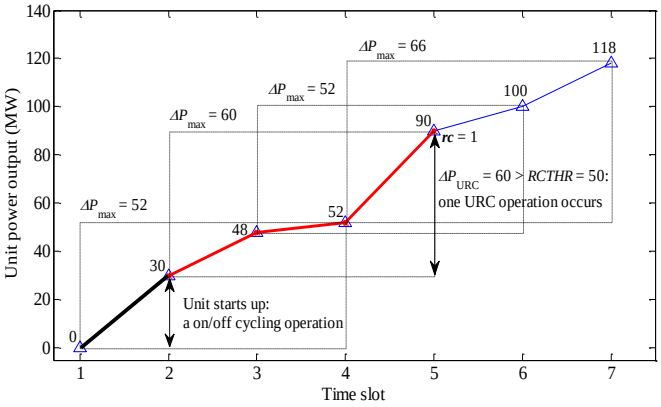

Fig. 1. Illustration of the URC operation. The 4-slot time windows for checking the URC operation are represented by the dash-line rectangles.

Fig. 1 illustrates the identification of the URC operation, where $RCTHR_i$ = 50MW and the URC operation shall be within a 4-slot time window. It can be seen that the maximum output change ($\Delta P_{\max}$) in a time window may not be identical to the output change that forms the URC operation (ΔP_{URC}). In the four time windows shown in Fig. 1, $\Delta P_{\max}$ = 52MW, 60MW, 52MW, and 66MW; correspondingly ΔP_{URC} = 22MW, 60MW, 10MW, and 28MW. Therefore, even if $\Delta P_{\max}$ exceeds the 50-MW URC threshold in all of the four windows, only one URC operation is formed in the second window.

C. Top-Level Scheduling Model

The NLVR contains numerous possible net load realizations. In response to each realization, the generators may incur some URC operations which cannot be avoided by properly distributing the cycling onus among the generators. The top-level scheduling model aims to minimize such URC operations by reshaping the NLVR via PEV power coordination. The detailed formulation of the top-level scheduling model is as follows:

$$\min \sum_{t\in T}\Big\{\sum_{i\in I}\theta_{rc}[rc_{i,t}^{\text{up}}+rc_{i,t}^{\text{down}}] + \sum_{i\in I}\theta_{fc}SW[\,fc_{i,t}(\bar{g}_{i,t})+fc_{i,t}(\underline{g}_{i,t})]-p_t^{\text{PEV}}SW\Big\} \tag{5}$$

subject to

1) Power balance constraints:

$$\sum_{i\in I}\bar{g}_{i,t}=L_t+p_t^{\text{PEV}}-\underline{W}_t^{\text{UI}},\ \forall t\in T \tag{6}$$

$$\sum_{i\in I}\underline{g}_{i,t}=L_t+p_t^{\text{PEV}}-\bar{W}_t^{\text{UI}},\ \forall t\in T \tag{7}$$

2) Generator power output limits:

$$U_{i,t}\underline{G}_i\le\bar{g}_{i,t}\le U_{i,t}\bar{G}_i,\ \forall t\in T,\forall i\in I \tag{8}$$

$$U_{i,t}\underline{G}_i\le\underline{g}_{i,t}\le U_{i,t}\bar{G}_i,\ \forall t\in T,\forall i\in I \tag{9}$$

3) Generator fuel cost function:

$$fc_{i,t}(g_{i,t})=a_iU_{i,t}+b_ig_{i,t}+c_ig_{i,t}^2,\forall t\in T,\forall i\in I \tag{10}$$

4) Conditions of URC operation:

$$\bar{g}_{i,t}-\underline{g}_{i,t-k}-LN\cdot rc_{i,t}^{\text{up}}\le RCTHR_i+LN\cdot[(k+1)-\sum_{r=0}^{k}U_{i,t-r}],\forall t\in T,\forall i\in I,\forall k=1\ldots WS-1 \tag{11}$$

$$\bar{g}_{i,t-k}-\underline{g}_{i,t}-LN\cdot rc_{i,t}^{\text{down}}\le RCTHR_i+LN\cdot[(k+1)-\sum_{r=0}^{k}U_{i,t-r}],\forall t\in T,\forall i\in I,\forall k=1\ldots WS-1 \tag{12}$$

5) Start-up and shut-down ramp rate limits:

$$\bar{g}_{i,t}\le SURL_i(U_{i,t}-U_{i,t-1})+\bar{G}_i(1-U_{i,t}+U_{i,t-1}),\ \forall t\in T,\forall i\in I \tag{13}$$

$$\bar{g}_{i,t}\le SDRL_i(U_{i,t}-U_{i,t+1})+\bar{G}_i(1-U_{i,t}+U_{i,t+1}),\ \forall t\in T,\forall i\in I \tag{14}$$

$$\underline{g}_{i,t}\le SURL_i(U_{i,t}-U_{i,t-1})+\bar{G}_i(1-U_{i,t}+U_{i,t-1}),\ \forall t\in T,\forall i\in I \tag{15}$$

$$\underline{g}_{i,t}\le SDRL_i(U_{i,t}-U_{i,t+1})+\bar{G}_i(1-U_{i,t}+U_{i,t+1}),\ \forall t\in T,\forall i\in I \tag{16}$$

6) System-level PEV power and energy constraints:

$$P_t^{\text{PEV\_dch}}\le p_t^{\text{PEV}}\le P_t^{\text{PEV\_ch}},\forall t\in T \tag{17}$$

$$E_t^{\text{PEV\_dch}}\le\sum_{t_n=1}^{t}p_{t_n}^{\text{PEV}}SW\le E_t^{\text{PEV\_ch}},\forall t\in T \tag{18}$$

7) Binary variable constraints:

$$rc_{i,t}^{\text{up}},rc_{i,t}^{\text{down}}\in\{0,1\},\ \forall t\in T,\forall i\in I \tag{19}$$

where $\bar{g}_{i,t}$, $\underline{g}_{i,t}$, p_t^{PEV}, $rc_{i,t}^{\text{up}}$, and $rc_{i,t}^{\text{down}}$ are the decision variables of the top-level scheduling model.

A URC operation is most likely to occur between two timeslots if the net load varies from the upper bound of the NLVR in one slot to the lower bound of the NLVR in the other, and vice versa. Thus, the generator power output in each timeslot of the scheduling horizon is represented by dual variables $\bar{g}_{i,t}$ and $\underline{g}_{i,t}$. The objective function (5) contains three objectives: to minimize the URC operations (the primary objective) with the least compromise in PEV charging energy (the secondary objective) while the generators are dispatched economically (the tertiary objective). Coefficients θ_{rc} and θ_{fc} are used to prioritize these three objectives and their ranges are as follows:

$$\theta_{rc}>\max\{P_t^{\text{PEV\_ch}}-P_t^{\text{PEV\_dch}}:t\in T\} \tag{20}$$

$$0<\theta_{fc}<0.5/\max\{ifc_i(\bar{G}_i):i\in I\} \tag{21}$$

where $ifc_i(\bar{G}_i)$ represents the incremental fuel cost of unit i at its maximum power output. $P_t^{\text{PEV\_ch}}-P_t^{\text{PEV\_dch}}$ represents the PEV power range in timeslot t. With θ_{rc} set to be greater than the maximum PEV power range in the scheduling horizon, reducing a URC operation will outweigh any possible increases in the PEV power. Thus, the primary objective is prioritized over the secondary one. With θ_{fc} satisfying (21), an increase in the PEV power, though leads to a higher generator fuel cost, will have an overwhelming effect on minimizing the objective function. Hence, the secondary objective is prioritized over the tertiary one. It shall be noted that if the true cost associated with the URC operation can be captured, the primary objective would merge with the tertiary one, forming a composite generator operating cost. Compared with the prioritized objectives in (5), minimizing the composite cost can further facilitate the economic operation of the system. However, quantifying the true URC cost is difficult. Analysis in [1] indicated that large variations in the costs of cycling exist not only between different unit types but also between individual units of each type. For example, from the 25th percentile estimate to the 75th percentile estimate of the URC cost for each unit type considered in [1], large variations can be observed which range from 98% to 305%. Compared with quantifying the true URC cost, identifying the units which are susceptible to cycling operations is relatively easy. Since the proposed scheme can protect the susceptible units from the URC operations, it can serve as a timely remedy to the increasingly severe URC problem.

In (17) and (18), the positive and negative values of p_t^{PEV} indicate the charging and discharging operations of PEVs, respectively. Constraint (17) defines the system-level PEV power range in each timeslot, and constraint (18) represents the system-level cumulative PEV energy limits. These two constraints can be determined by aggregating the information of individual PEVs. This paper assumes that the information reporting mechanism proposed in [22] is used to realize the information aggregation. Each PEV user will report his anticipated charging activities to his regional PEV aggregator. The reported information includes the expected plug-in and plug-out time, the rated charging/discharging power of the

PEV battery, the uncontrolled charging power profile leading to the desired battery SOC, and the maximum discharging power profile leading to minimum allowable SOC. It shall be noted that the reported charging plans do not have to be very accurate. In fact, routine charging schedule is already good enough to approximate charging plan for most of the commuter PEVs. The system-level PEV power range and energy limits are determined as follows:

$$P_t^{\text{PEV\_ch}} = \sum_{A_k \in AI} \sum_{e \in A_k} PIPO_{e,t} R_e^{\text{ch}} / \eta_e \tag{22}$$

$$P_t^{\text{PEV\_dch}} = -\sum_{A_k \in AI} \sum_{e \in A_k} PIPO_{e,t} \eta_e R_e^{\text{dch}} \tag{23}$$

$$E_t^{\text{PEV\_ch}} = \sum_{t_n=1}^{t} \sum_{A_k \in AI} \sum_{e \in A_k} R_{e,t_n}^{\text{unctl\_ch}} / \eta_e \cdot SW \tag{24}$$

$$E_t^{\text{PEV\_dch}} = \sum_{t_n=1}^{t} \sum_{A_k \in AI} \sum_{e \in A_k} R_{e,t_n}^{\text{max\_dch}} \eta_e SW \tag{25}$$

In (22) and (23), R_e^{ch} and R_e^{dch} are battery-side quantities, whereas $P_t^{\text{PEV\_ch}}$ and $P_t^{\text{PEV\_dch}}$ are grid-side quantities. To refer R_e^{ch} and R_e^{dch} to the grid side to calculate $P_t^{\text{PEV\_ch}}$ and $P_t^{\text{PEV\_dch}}$, the charger efficiency η_e should be considered in (22) and (23). In (24), $R_{e,\,t_n}^{\text{unctl\_ch}}$ is the charging power received by the PEV *e*'s battery in timeslot t_n when the charging is uncontrolled. In (25), $R_{e,\,t_n}^{\text{max\_dch}}$ is the discharging power delivered from the PEV *e*'s battery in timeslot t_n in the scenario that starting from the plug-in of PEV *e*, the PEV battery is being discharged at its maximum rate until the minimum allowable SOC is reached. The uncontrolled charging power profile $\{R_{e,\,t_n}^{\text{unctl\_ch}}\}$ and the maximum discharging power profile $\{R_{e,\,t_n}^{\text{max\_dch}}\}$ represent the fastest charging and discharging processes of PEV *e*, respectively. Thus, according to (24) and (25), $E_t^{\text{PEV\_ch}}$ and $E_t^{\text{PEV\_dch}}$ represent the maximum amount of energy that can be charged to and discharged from the PEVs from the 1st to the t^{th} timeslot of the scheduling horizon, respectively. $E_t^{\text{PEV\_ch}}$ and $E_t^{\text{PEV\_dch}}$ form the envelope for feasible trajectories of the cumulative PEV energy. Therefore, the PEV power is flexible to be controlled as long as the resultant cumulative energy trajectory complies with constraint (18).

It should be pointed out that $E_t^{\text{PEV\_ch}}$ and $E_t^{\text{PEV\_dch}}$ can be altered by the actual cumulative energy trajectory. According to constraint (18), at the grid side, an amount of charging energy E^{ch} can be offset by an equal amount of discharging energy $E^{\text{dch}} = -E^{\text{ch}}$, or vice versa. However, when referred to the battery side, the received charging energy is $E^{\text{ch}}\eta_e$, and the offsetting discharging energy required is $-E^{\text{ch}}\eta_e$, which is equivalent to $-E^{\text{ch}}\eta_e^2$ at the grid side. Therefore, at the grid side an amount of charging energy can actually be offset by a smaller amount of discharging energy. This indicates that a charging operation has an effect of raising the lower boundary of the cumulative PEV energy $E_t^{\text{PEV\_dch}}$ in the subsequent timeslots (Note that $E_t^{\text{PEV\_dch}}$ is negative, so raising $E_t^{\text{PEV\_dch}}$ reduces its magnitude.). Similarly, because offsetting an amount of discharging energy E^{dch} requires a larger amount of charging energy $-E^{\text{dch}}/\eta_e^2$, a discharging operation has an effect of raising the upper boundary of the cumulative PEV energy $E_t^{\text{PEV\_ch}}$ in the subsequent timeslots. Nevertheless, constraint (18) uses unaltered $E_t^{\text{PEV\_ch}}$ and $E_t^{\text{PEV\_dch}}$, and thus is an approximation to the precise constraint of the cumulative PEV energy. The approximation is considered adequate for the proposed scheme in most cases based on the following reasoning. As the secondary objective of the proposed scheme is to maximize the PEV charging energy, the PEV power trajectory resulting from the proposed scheme would mainly consist of charging operations. Though a number of charging operations may saliently raise $E_t^{\text{PEV\_dch}}$, the resultant cumulative energy trajectory is normally a trajectory of charging energy which stays positive and away from $E_t^{\text{PEV\_dch}}$. Thus, there is little risk of the cumulative energy trajectory generated by the proposed scheme violating the actual $E_t^{\text{PEV\_dch}}$. In fact, $E_t^{\text{PEV\_dch}}$ is normally a nonbinding constraint for a PEV power trajectory dominated by charging operations; hence, using the unaltered $E_t^{\text{PEV\_dch}}$ in constraint (18) shall have little impact on the PEV power dispatch results of the proposed scheme. Since the discharging operation is often a minority in the PEV power trajectory generated by the proposed scheme, $E_t^{\text{PEV\_ch}}$ will only be slightly raised. Hence, the unaltered $E_t^{\text{PEV\_ch}}$ in constraint (18) can serve as an adequate approximation to the precise $E_t^{\text{PEV\_ch}}$ in most cases without adversely affecting the validity of the results. Nevertheless, the precise cumulative energy constraint may be needed in some cases, for example, when there are lots of discharging operations in the PEV power trajectory. Either of the two methods proposed in [23] and [24] can be adopted for obtaining the precise $E_t^{\text{PEV\_ch}}$ and $E_t^{\text{PEV\_dch}}$. The first method is to continuously update the charging constraints of individual PEVs to reflect the impact of charging/discharging operations on $E_t^{\text{PEV\_ch}}$ and $E_t^{\text{PEV\_dch}}$. The second method is to distinguish the charging and discharging operations by using two variables such that the charging operation's impact on $E_t^{\text{PEV\_dch}}$ and the discharging operation's impact on $E_t^{\text{PEV\_ch}}$ can be considered separately.

There are two points worth noting about the top-level scheduling model. First, the term $LN\sum_{h=1}^{k-1} rc_{i,t-h}$, which is included in (4) to avoid double-counting the URC operation, is absent from the URC conditions (11) and (12). This is because in the top-level scheduling model all net load scenarios in the NLVR are considered possible. Thus, one URC operation caused by a net load scenario should not deny the possibility of any other URC operation caused by another net load scenario. Second, no ramp rate constraints are imposed on the generator power outputs. This is because establishing ramp rate constraints between $\overline{g}_{i,t-1}$ and $\underline{g}_{i,t}$ as well as $\underline{g}_{i,t-1}$ and $\overline{g}_{i,t}$ would force a lot more generators to be committed to provide sufficient ramping capacity for handling the steepest possible net load ramp between two adjacent timeslots. In fact,

according to the historical data used in this paper, 99.95% of the actual net load ramps between two adjacent timeslots are not as half steep as their corresponding steepest possible ramps. Fig. 2 shows the distribution of the historical data of net load ramps between two adjacent timeslots.

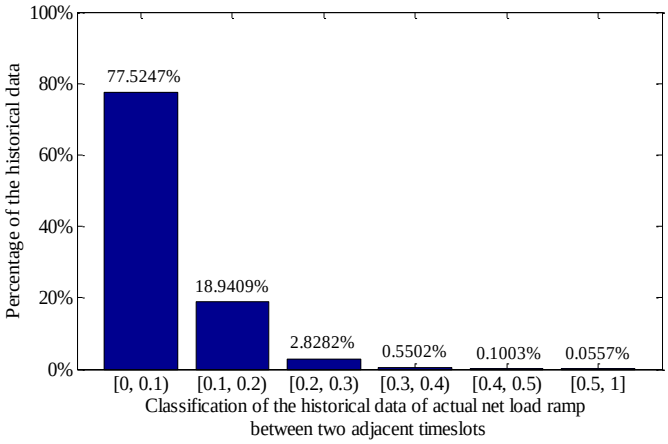

Fig. 2. Distribution of the historical data of net load ramps between two adjacent timeslots. The data are represented as percentages of their corresponding steepest possible ramps in the NLVR.

D. Middle-Level Dispatch Model

The top-level scheduling model takes into account all possible net load scenarios in the NLVR including those extremely varying ones. As a result, the PEV power can be intensely used to reshape the NLVR, leading to a severe compromise in fulfilling the charging demand. Based on the latest update of WP forecasts, the middle-level dispatch model will exempt over-scheduled anti-URC regulation onus on PEVs to promote PEV charging.

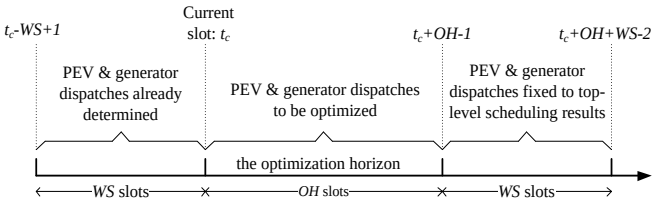

Fig. 3. Schematic of the dispatch horizon of the middle-level dispatch model

The dispatch model is solved in a rolling fashion for each timeslot. The dispatch horizon is shown in Fig. 3. From the current timeslot t_c to t_c+*OH*-1 is the optimization horizon. When the PEV and generator dispatches in t_c are optimized, the dispatches in each of the remaining *OH*-1 timeslots in the optimization horizon will be optimized as well, yet, only the dispatches in t_c will be actually deployed. As the dispatch model rolls forward, the WP forecasts are assumed to be iteratively updated with gradually diminished uncertainties [25] as follows:

$$\overline{W}_{t_c+n}^{\text{UI\_upd}} = W_{t_c+n}^{\text{a}} + n/(NUF+1)(\overline{W}_{t_c+n}^{\text{UI}} - W_{t_c+n}^{\text{a}}) \quad (26)$$

$$\underline{W}_{t_c+n}^{\text{UI\_upd}} = W_{t_c+n}^{\text{a}} + n/(NUF+1)(\underline{W}_{t_c+n}^{\text{UI}} - W_{t_c+n}^{\text{a}}) \quad (27)$$

where $n=0\ldots NUF$. Beyond t_c+*NUF*, the WP uncertainty intervals remain the same as those used in the top-level scheduling model. *OH* is set to *NUF*+1 such that the dispatch model will take all updated WP forecasts into consideration.

Two *WS*-slot time windows are attached to the optimization horizon: one from the current timeslot t_c back to t_c-*WS*+1, and the other from t_c+*OH*-1 to t_c+*WS*+*OH*-2. These two time windows are used for the dispatch model to take into account the URC operations formed across the boundaries of the optimization horizon, e.g. between t_c-1 and t_c+1 across t_c, or between t_c+*OH*-2 and t_c+*OH* across t_c+*OH*-1. Dispatches in the past timeslots ([t_c-*WS*+1, t_c-1]) will be fixed to the earlier solutions of the dispatch model, while dispatches in the timeslots beyond the optimization horizon ([t_c+*OH*, t_c+*OH*+*WS*-2]) will adhere to the solution of the top-level scheduling. Timeslots in [t_c+*OH*, t_c+*OH*+*WS*-2] can also be included in the optimization horizon. However, extending the optimization horizon beyond t_c+*OH*-1 is not really necessary, as simulations have shown that extending the optimization horizon into [t_c+*OH*, t_c+*OH*+*WS*-2] would only have little impact on the dispatch results.

The middle-level dispatch model comprises objective function (5) and constraints (6)-(19) with similar formulation to the top-level scheduling model but the following four main differences. First, according to (26) and (27), the actual WP in the current timeslot t_c is assumed to be revealed, i.e. $\overline{W}_{t_c}^{\text{UI\_upd}} = \underline{W}_{t_c}^{\text{UI\_upd}} = W_{t_c}^{\text{a}}$. Hence, the upper and lower bounds of the NLVR in t_c will coincide, and correspondingly, the dual generator power output variables $\overline{g}_{i,t_c}$ and $\underline{g}_{i,t_c}$ in the top-level scheduling model would become a single variable g_{i,t_c} in the mid-level dispatch model.

Second, between timeslots *t*-*k* and *t*, if there are any intermediate timeslots *t*-*h* (*t*-*k*<*t*-*h*<*t*) belonging to [t_c-*WS*+1, t_c], which is the set of timeslots in the dispatch horizon with deterministic generator power outputs, the URC conditions regarding *t*-*k* and *t* will have the term $LN\sum_{h=1}^{k-1} rc_{i,t-h}$ included to avoid double-counting the URC operation. Such URC conditions in the dispatch model are summarized as follows. Between the current timeslot t_c and a past timeslot:

$$\begin{aligned} &g_{i,t_c} - g_{i,t_c-k} - LN\cdot rc_{i,t_c}^{\text{up}} \le RCTHR_i \\ &+LN[(k+1) - \sum_{r=0}^{k} U_{i,t_c-r}] + LN\sum_{h=1}^{k-1}(rc_{i,t_c-h}^{\text{up}} + rc_{i,t_c-h}^{\text{down}}), \\ &\forall i \in I, \forall k = 2\ldots WS-1 \end{aligned} \quad (28)$$

$$\begin{aligned} &g_{i,t_c-k} - g_{i,t_c} - LN\cdot rc_{i,t_c}^{\text{down}} \le RCTHR_i \\ &+LN[(k+1) - \sum_{r=0}^{k} U_{i,t_c-r}] + LN\sum_{h=1}^{k-1}(rc_{i,t_c-h}^{\text{up}} + rc_{i,t_c-h}^{\text{down}}), \\ &\forall i \in I, \forall k = 2\ldots WS-1 \end{aligned} \quad (29)$$

Between a future timeslot and a past timeslot:

$$\begin{aligned} &\overline{g}_{i,t} - g_{i,t-k} - LN\cdot rc_{i,t}^{\text{up}} \le RCTHR_i \\ &+LN\cdot(k+1-\sum_{r=0}^{k} U_{i,t-r}) + LN\sum_{h=t-t_c}^{k-1}(rc_{i,t-h}^{\text{up}} + rc_{i,t-h}^{\text{down}}), \\ &\forall i \in I, \forall t \in [t_c+1, t_c+WS-2], \forall k \in [t-t_c+1, WS-1] \end{aligned} \quad (30)$$

$$\begin{aligned} &g_{i,t-k} - \underline{g}_{i,t} - LN\cdot rc_{i,t}^{\text{down}} \le RCTHR_i \\ &+LN\cdot(k+1-\sum_{r=0}^{k} U_{i,t-r}) + LN\sum_{h=t-t_c}^{k-1}(rc_{i,t-h}^{\text{up}} + rc_{i,t-h}^{\text{down}}), \\ &\forall i \in I, \forall t \in [t_c+1, t_c+WS-2], \forall k \in [t-t_c+1, WS-1] \end{aligned} \quad (31)$$

Third, if the updated WP uncertainty intervals in two adjacent timeslots of the optimization horizon satisfy the following condition:

$$\begin{cases} \bar{W}_{t_c+g}^{\text{UI\_upd}} - \underline{W}_{t_c+g}^{\text{UI\_upd}} \le 0.5(\bar{W}_{t_c+g}^{\text{UI}} - \underline{W}_{t_c+g}^{\text{UI}}) \\ \bar{W}_{t_c+g+1}^{\text{UI\_upd}} - \underline{W}_{t_c+g+1}^{\text{UI\_upd}} \le 0.5(\bar{W}_{t_c+g+1}^{\text{UI}} - \underline{W}_{t_c+g+1}^{\text{UI}}) \end{cases} \tag{32}$$

then ramp rate limits will be imposed between the generator power outputs in t_c+g and t_c+g+1.

Fourth, due to the limited number of timeslots covered by the optimization horizon, the dispatch model would have the risk of overly restoring the PEV charging power. Consequently, the anti-URC regulation capacity reserved by PEVs may become insufficient for the timeslots beyond the optimization horizon, and the effectiveness of the PEV-aided URC operation mitigation can be jeopardized. To limit the over restoration, the reshaped NLVR from the top-level scheduling, which has strong mitigating effect on URC operations, is used in the dispatch model to confine the updated NLVR in each timeslot of the optimization horizon as follows:

$$L_t + P_t^{\text{PEV\_sched}} - \underline{W}_t^{\text{UI}} \ge L_t + p_t^{\text{PEV}} - \underline{W}_t^{\text{UI\_upd}}, \quad \forall t \in [t_c, t_c + OH - 1] \tag{33}$$

$$L_t + P_t^{\text{PEV\_sched}} - \bar{W}_t^{\text{UI}} \le L_t + p_t^{\text{PEV}} - \bar{W}_t^{\text{UI\_upd}}, \quad \forall t \in [t_c, t_c + OH - 1] \tag{34}$$

such that the PEV charging power restoration will depend on the improvement in the WP forecast.

E. Bottom-Level PEV Charging Control Strategy

At the bottom level, the decentralized PEV charging control strategy previously devised in [26] is used to guide PEVs to implement the PEV power dispatch instruction from the middle-level dispatch model. In this decentralized charging control strategy, each PEV will autonomously determine its power based on a real-time directing signal (DS) and its own urgency level of charging (ULOC).

The ULOC is defined as a function of the PEV battery capacity and PEV charging margin. The charging margin is the difference between the battery capacity that can be fulfilled before the planned departure time and the battery capacity to be fulfilled from the current SOC to the desired SOC. The ULOC is calculated as follows:

$$\mu_{e,t} = C_e^{\text{batt}} / (R_e^{\text{ch}}(DT_e - t) / C_e^{\text{batt}} - (SOC_e^{\text{desired}} - SOC_{e,t})) \tag{35}$$

It shall be noted that if $\mu_{e,t}$ exceeds its preset upper limit $\mu_e^{\max}$ or becomes negative, it will be fixed to $\mu_e^{\max}$, which is set to $100C_e^{\text{batt}}$ in this paper.

The real-time DS is generated at an information hub. The hub communicates with the system control center and PEV aggregators to obtain the PEV power dispatch instruction and the actual PEV power. The DS is calculated as follows:

$$ds_{t+nd} = DI_t^{\text{PEV}} / \left|DI_t^{\text{PEV}}\right| \cdot \left|ds_{t+(n-1)d} + \beta(p_{t+(n-1)d}^{\text{PEV}} - DI_t^{\text{PEV}})\right| \tag{36}$$

The sign of DS follows that of the PEV power dispatch instruction, indicating the need for grid-to-vehicle (G2V) (+) or vehicle-to-grid (V2G) (−) power. The DS is updated in each sub-timeslot *d*, and then broadcasted to all PEVs.

Upon receiving the DS, each PEV will determine its power as follows:

$$r_{e,t+nd} = \begin{cases} \min\{R_e^{\text{ch}},\ \mu_{e,t} / ds_{t+nd}\}, & ds_{t+nd} > 0 \\ \max\{\mu_{e,t}^{-1} / ds_{t+nd}, -R_e^{\text{dch}}\}, & ds_{t+nd} < 0 \end{cases} \tag{37}$$

As can be seen from (37), the PEV power is in direct proportion to the PEV's ULOC when the DS is positive, whereas it is in inverse proportion to the ULOC when the DS is negative. This indicates that a PEV with higher ULOC will have higher charging priority and less discharging onus assumed, and vice versa. Thus, the resultant power distribution among PEVs will be in favor of satisfying the heterogeneous PEV charging requirements. Moreover, a maximum SOC limit can be incorporated into this charging control strategy to further promote the fulfillment of PEV charging requirements. Specifically, a maximum SOC limit is set for each PEV, which is slightly higher than the desired SOC. For a PEV that has reached its maximum SOC limit, if the DS is positive, the PEV will stop responding to the DS and take zero charging power. As a result, the PEVs which have not yet fulfilled their charging requirements can receive more charging energy to speed up their charging processes.

Fig. 4 is an overall flowchart of the proposed hierarchical scheme for a scheduling horizon of one day. It clarifies how the models at the top, middle, and bottom levels are linked up and work together, and suggests the solving algorithm for each model. It is worth mentioning that the proposed scheme can be fitted in a three-segment power market composed of day-ahead market, intra-day markets, and real-time spot market. The top-level scheduling will be performed in the day-ahead market based on initial forecasts of net load. The middle-level dispatches will be determined in the intra-day markets, which allow the market participants to make decisions closer to real-time so that updated forecasts can be considered in fine-tuning the day-ahead schedule; the intra-day market is repeated for each timeslot of the day to finalize the PEV and generator dispatches. The bottom-level charging control strategy can be used to provide balancing services in the real-time spot market. While the technical content of the proposed scheme is the focus here, detailed framework for the application of the proposed scheme in a market environment will be investigated in the future.

III. Benchmark Scheme

A benchmark scheme is developed from the BESS control methods proposed in [11] and [12] to control the PEV power to hedge against the URC operations. In the benchmark scheme, PEVs reserve upward and downward regulation capacities by being charged at power levels lower than their rated charging power. The partial charging power level is termed as the PEV base power level and represented as a fraction of the rated power. At the scheduling stage of the benchmark scheme, the objective is to find the PEV base power level at which PEVs reserve sufficient anti-URC regulation capacity. A series of simulations are conducted to

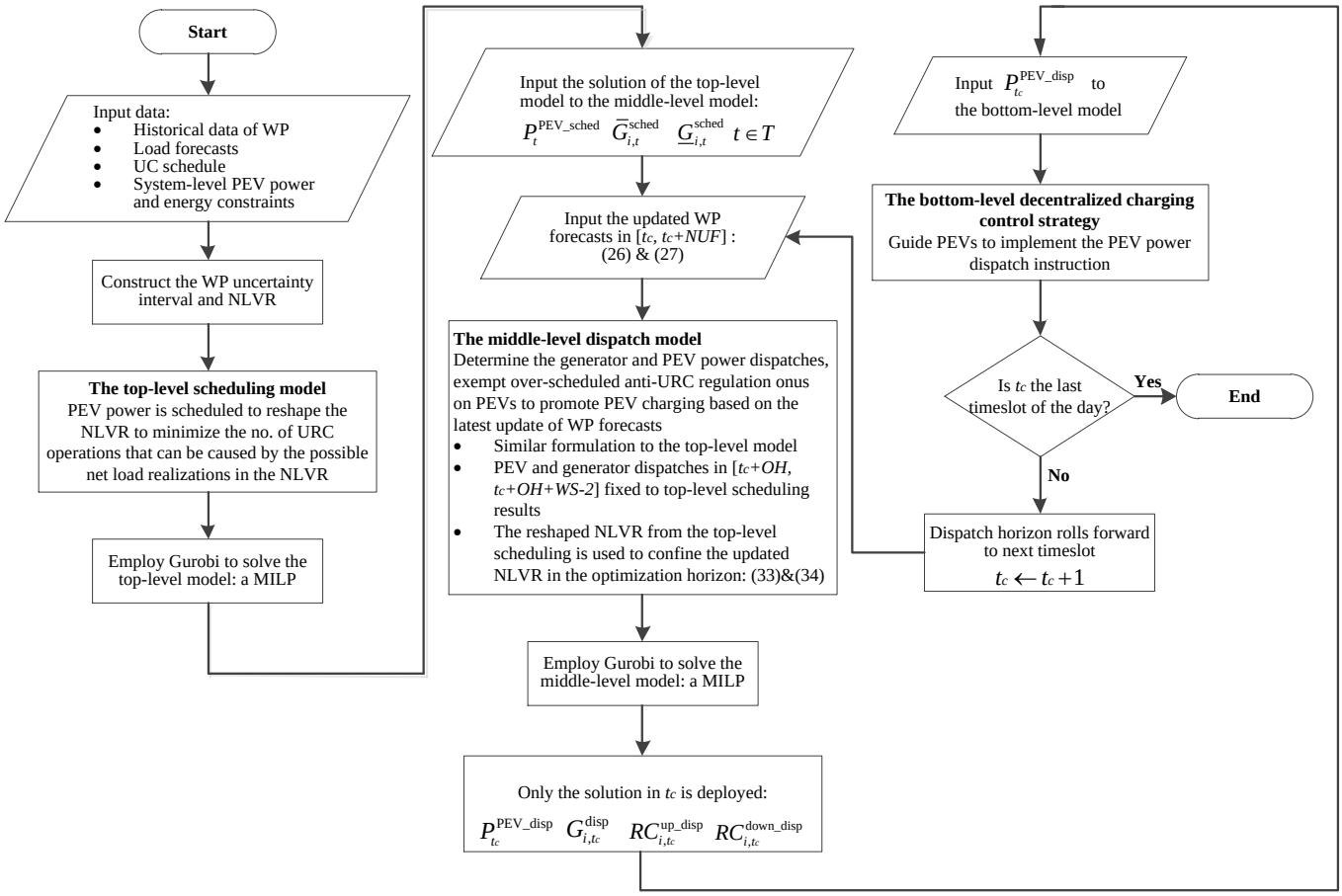

Fig. 4. Flowchart of the proposed hierarchical scheme for a scheduling horizon of one day.

search through different PEV base power levels. Point predictions of WP are considered in the simulations. For each PEV base power level δ, say 70% of the rated power, the benchmark scheme first determines the minimum anti-URC regulation power required in each timeslot, and then the determined regulation power is added to the PEV base power level. The resultant PEV power profile is adjusted to comply with the PEV power and energy constraints in (17) and (18). The adjusted PEV power profile is the one that provides the anti-URC regulation. By examining how many URC operations still persist after the adjusted PEV power profile is implemented, how sufficient the regulation capacity reserved by PEVs at base power level δ can be evaluated.

The dispatch process of the benchmark scheme takes into account the updated WP forecasts and rolls forward through each timeslot to determine the minimum anti-URC regulation power required. PEVs, which are charged at the base power level, will implement as much of the required regulation power as possible in each timeslot without violating (17) and (18).

IV. Simulation Setting

The simulation is conducted over an 81-hour scheduling horizon, which contains 324 15-min timeslots (SW = 0.25 hr). WP and system load are updated once every 15 minutes and assumed to be constant within each 15-min timeslot.

The test system consists of 9 coal-fired units and 7 gas-fired units. Generator parameters are obtained from [27] and [28] and summarized in Table I. The threshold $RCTHR_i$ is set to 20% of the generator's dependable capacity [1]. As there is no published data on the time span of a URC operation, it is assumed that the maximum span of a URC operation is 12 timeslots (WS = 12). The large constant LN is set to 1000.

The historical data of forecasted and actual WP from the aggregate Belgian wind farms in 2013 [29] are used to construct 40 WP uncertainty intervals with 96% confidence level (i.e. $Q\%$ = 96%). The predicted and actual WP profiles of the aggregate Belgian wind farms from 15:15 6/3/2014 to 00:15 10/3/2014 are used in the simulation, as shown in Fig. 5(a). For further investigation of the performance of the proposed scheme in an extreme scenario of WP intermittency, a hypothetical WP profile containing severe fluctuations is also considered in the simulation, as shown in Fig. 5(b). In the dispatch process, updated WP forecasts are assumed to be available in timeslots [t_c, t_c+22]. The non-PEV load is shown in Fig. 6, which is the downscaled load profile of New South Wales from 15:15 1/June/2014 to 00:15 5/June/2014 [30]. The magnitudes of WP and load forecast errors are shown in Fig. 7. It can be seen that the load forecast errors are relatively insignificant compared with the WP forecast errors. Thus, the WP uncertainty is the dominant contributor to the net load uncertainty, and here the non-PEV load is assumed to be deterministic.

TABLE I
GENERATOR PARAMETERS

Unit	Type 1	Type 2	Type 3
Fuel type	Coal	Coal	Gas
No. of units	5	4	7
$\overline{G}_i$, $\underline{G}_i$ (MW)	350, 140	155, 56	150, 42
RUL_i, RDL_i (MW/min)	4, 4	3, 3	2.5, 2.5
$SURL_i$, $SDRL_i$ (MW)	150, 150	65, 65	90, 90
$RCTHR_i$ (MW)	70	31	30
a_i (10^{-3} \$/MW^{2}h)	7.86	13.41	14.26
b_i (\$/MWh)	17.91	18.19	49.67
c_i (\$/h)	779.7	444.5	1013

A total number of 240,000 PEVs is considered in the simulation. Each PEV has one of the following battery capacities: 16.5 kWh, 24 kWh, and 60 kWh, corresponding to 1.8 kW, 1.8 kW and 6.6 kW chargers, respectively. PEV plug-in and plug-out time are sampled from two distributions models based on a U.S. national survey on personal driving patterns [31], which characterizes the daily start time of the first trip and the end time of the last trip of U.S. private cars [22]. The charger efficiency is set to 90%. The initial SOC is uniformly distributed between 15% and 80%, and the desired SOC is assumed to be 90%.

In the bottom-level decentralized charging control strategy, the individual PEV power is assumed to be determined once every 30 s according to (37). β in (36) affects the pace of PEV power adjustment. Depending on the rate of change of the PEV power dispatch instruction and the number of PEVs, the choice of suitable value for β may vary. In this paper, simulations showed that a value of β in the range of 0.001–0.006 works well. Thus, β is set to 0.002. Since the desired SOC is assumed to be 90%, it is stipulated that the PEV would stop responding to the positive DS when its SOC reaches 91%, i.e. the maximum SOC limit is set to 91%.

V. SIMULATION RESULTS AND DISCUSSIONS

A. Simulation with Realistic Wind Power Profile

In addition to the proposed hierarchical scheme and the benchmark scheme, two more schemes are tested. The first one assumes uncontrolled PEV charging. It helps to evaluate to what extent proper generator dispatches alone can avoid the URC operations. The second one is a deterministic version of the proposed scheme, in which point predictions of WP are adopted and the NLVR is replaced by a deterministic net load profile. The deterministic scheme shows how the lack of consideration for WP uncertainty would influence the URC operation mitigation. The performances of these four schemes will be compared in terms of the URC operation reduction and the preservation of PEV charging energy. The simulation is conducted with realistic WP profiles as shown in Fig. 5(a). All the optimizations are solved using Gurobi Optimizer 5.6.3 [32]. For convenience, figures in this section are generated as smooth line plots instead of stair-step graphs.

In Fig. 8, the NLVR with uncontrolled PEV charging is compared with the one generated by the top-level scheduling model of the proposed scheme (i.e. the reshaped NLVR). Apparently, the reshaped NLVR is much flatter. Take the

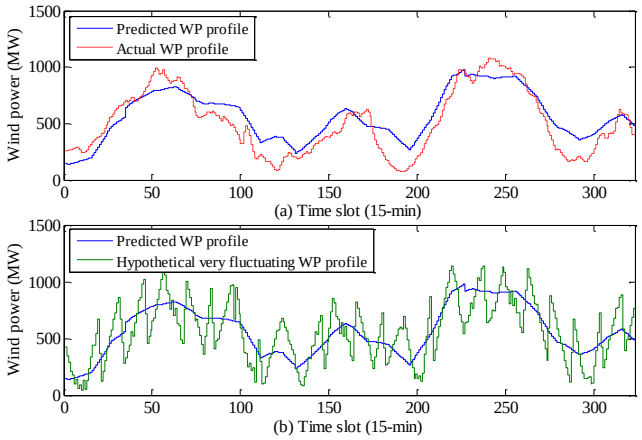

Fig. 5. WP profiles used in the simulation. (a) realistic WP scenario; (b) hypothetical very fluctuating WP scenario.

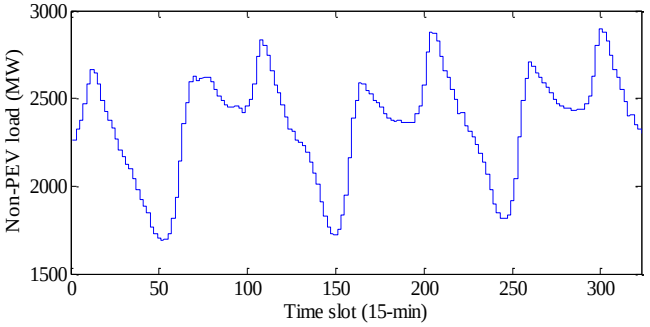

Fig. 6. Non-PEV load profile.

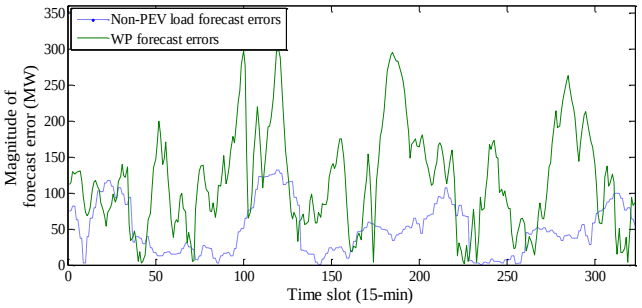

Fig. 7. Magnitude of WP and non-PEV load forecast errors.

predicted WP profile in Fig. 5(a) as an example WP realization; the correspondingly realized net load profiles are plotted in red in Fig. 8. As expected, the net load profile in the reshaped NLVR is considerably less varying than the other one. This shows that the reshaped NLVR do have stronger resistance to WP variations. This is because when reshaping the NLVR to minimize the possible URC operations, the top-level scheduling of the proposed scheme has taken into account the extremely varying net load scenarios in the NLVR. Thus, the top-level scheduling is conservative, and the reshaped NLVR often comes with a significant compromise in fulfilling the PEV charging demand. In fact, 53.72% of the charging demand can be unfulfilled following the scheduled PEV power profile from the top-level scheduling model of the proposed scheme.

The dispatched net load profiles and their standard deviations are shown in Fig. 9. The number of URC operations is summarized in Table II. With uncontrolled PEV charging, generators undergo dozens of URC operations;

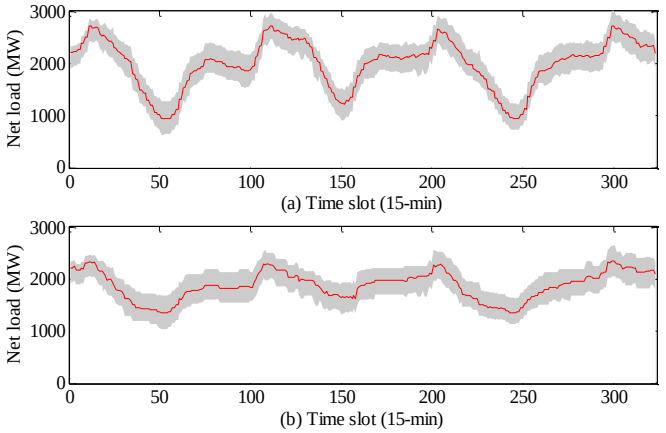

Fig. 8. (a) NLVR with uncontrolled PEV power, (b) reshaped NLVR from the top-level scheduling of the proposed scheme. The red solid lines represent the net load profiles corresponding to the predicted WP profile in Fig. 5(a).

whereas with controlled PEV charging, majority of URC operations are alleviated by either the benchmark scheme or the deterministic scheme, and the proposed scheme even manages to avert the URC operations completely. Thus, it can be seen that generator dispatches alone only have fairly limited mitigating effect on the URC operation.

TABLE II
NO. OF URC OPERATIONS CAUSED BY THE FOUR INVESTIGATED SCHEMES IN THE REALISTIC WP SCENARIO

Scheme	1	2	3	4
Upward URC	21	0	3	1
Downward URC	20	0	6	2
Total URC	41	0	9	3

Scheme 1–4 are the scheme with uncontrolled PEV charging, the proposed scheme, the benchmark scheme, and the deterministic scheme, respectively.

The benchmark scheme fails to mitigate multiple URC operations because of the insufficient anti-URC regulation capacity reserved in the PEVs at its scheduling stage. This insufficiency is caused by the WP uncertainty not being considered in the benchmark scheme. As can be seen from Fig. 10(a), in timeslots 67–69 where two upward URC operations occur, the PEV power controlled by the benchmark scheme hits its lower limit while the intended PEV power is beyond that limit. This exemplifies that the intended PEV power dispatch of the benchmark scheme cannot be completely implemented at times as a result of the insufficient regulation capacity in PEVs.

Another problem of the benchmark scheme is that it determines the required anti-URC regulation power without considering the regulation capacity of PEVs. Thus, the determined regulation power can concentrate in a short period, which could easily saturate the PEV power range. As shown in Fig. 10(b), the anti-URC regulation power determined by the benchmark scheme mainly concentrate in timeslots 62–79, while that determined by the proposed scheme spreads over the entire selected period from timeslot 30 to 80. The proposed scheme expands the downward regulation capacity of PEVs in the valley period of the net load from timeslot 30 to 60 such that the rapidly increasing net load in the subsequent timeslots 60–67 can be compensated adequately to avoid the upward

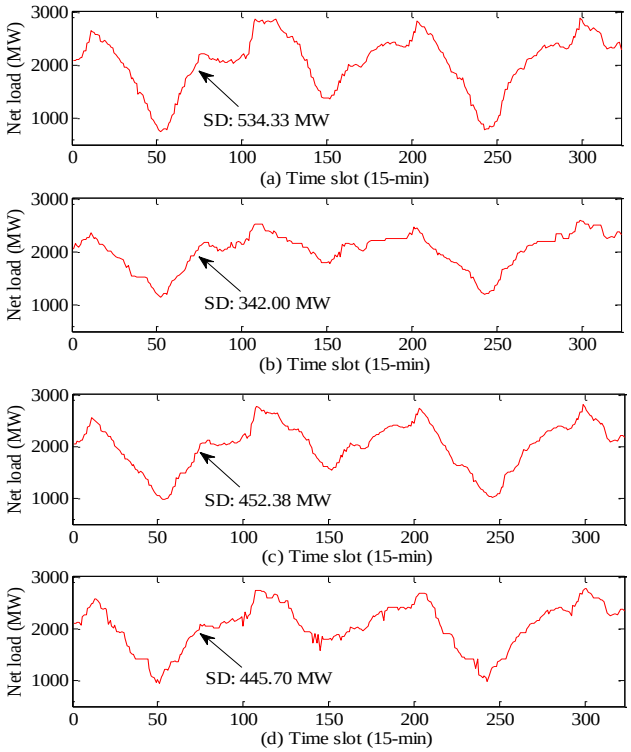

Fig. 9. Dispatched net load profiles in the realistic WP scenario. (a) with uncontrolled PEV charging; (b) the proposed scheme; (c) the benchmark scheme; (d) the deterministic scheme. SD stands for standard deviation.

URC operations.

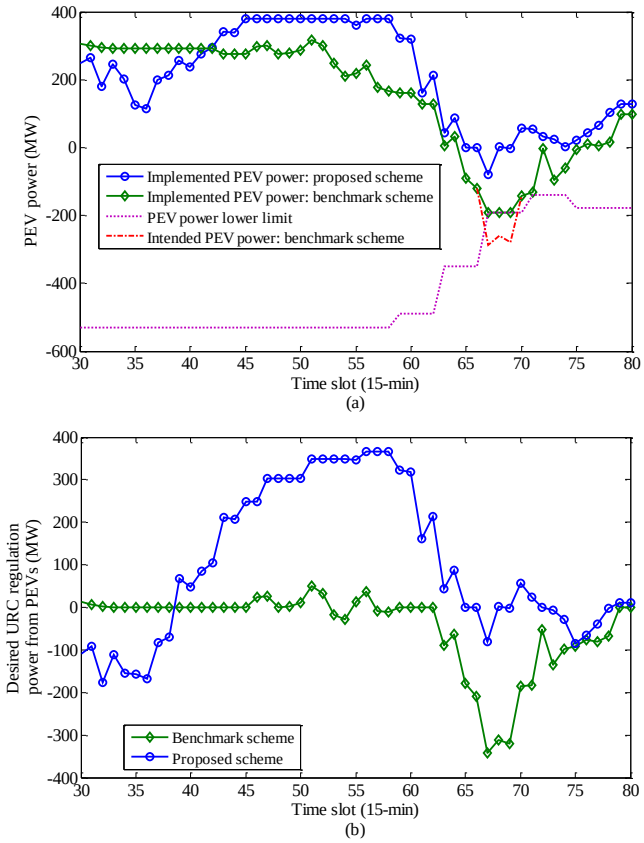

Fig. 10. Zoomed-in comparison between the dispatch results of the benchmark scheme and those of the proposed scheme, in the realistic WP scenario. (a) implemented and intended PEV power dispatch; (b) requested anti-URC regulation power from PEVs.

For the deterministic scheme, the lack of consideration for WP uncertainty also accounts for the scheme's failure to completely mitigate the URC operation. Not considering WP uncertainty causes the requested anti-URC regulation power to be underestimated. Consequently, the deterministic scheme can over-restore the PEV charging power. The two downward URC operations which the deterministic scheme failed to mitigate occur in timeslot 222 and 223. As shown in Fig. 11(a), the deterministic scheme actually attempted to avoid these two downward URC operations by increasing the PEV power in timeslots 217–223. Nevertheless, there has been insufficient upward regulation capacity reserved in PEVs due to the high-level charging power in the antecedent timeslots 200–216. On the other hand, the PEV power controlled by the proposed scheme remains at a significantly lower level during timeslots 200–216 such that sufficient upward regulation capacity can be prepared for the following net load decrease. This comparison shows that the PEV charging power has been overly restored by the deterministic scheme.

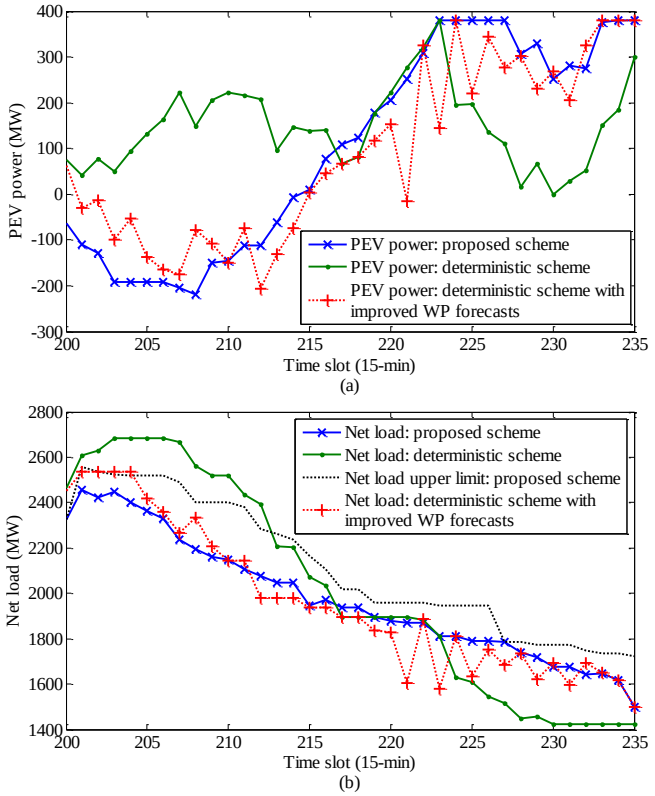

Fig. 11. Zoomed-in comparison between the dispatch results of the deterministic scheme and those of the proposed scheme, in the realistic WP scenario. (a) PEV power; (b) system net load.

To further illustrate the lack of consideration for WP uncertainty being responsible for the over restoration of PEV power in the deterministic scheme, the scheme is re-simulated with *NUF* increased from 22 to 35, which gives reduced WP uncertainty. The result is that the deterministic scheme manages to mitigate all URC operations. As shown in Fig. 11(a), with the reduced WP uncertainty, the new PEV power profile of the deterministic scheme is significantly decreased in timeslots 200–216 and the original PEV power over restoration is prevented. The new PEV power profile turns out to be similar to that produced by the proposed scheme. Therefore, in controlling PEV power to hedge against the URC operations, the proposed scheme is as effective as the deterministic scheme using more advanced WP forecasting techniques.

TABLE III
PEV CHARGING ENERGY LOSSES CAUSED BY THE FOUR INVESTIGATED SCHEMES IN THE REALISTIC WP SCENARIO

Scheme	1	2	3	4
CEL at scheduling stage	0%	53.72%	17.59%	1.62%
CEL in actual dispatch	0%	10.90%	19.80%	3.54%

Scheme 1–4 are the scheme with uncontrolled PEV charging, the proposed scheme, the benchmark scheme, and the deterministic scheme, respectively.

The PEV charging energy losses (CELs) are summarized in Table III and presented as percentages of the desired amount of charging energy. The CEL of a PEV is calculated by subtracting the actual amount of charging energy received by the PEV from its desired amount of charging energy. The results in Table III are the sum of individual PEVs' CELs. Since Scheme 1 assumes uncontrolled PEV charging, it incurs zero CELs. With no mechanisms to promote PEV charging, the benchmark scheme incurs the most CEL. The deterministic scheme is the best in minimizing the CEL. As for the proposed scheme, the CEL has been considerably reduced from 53.72% at the scheduling stage to 10.9% in the actual dispatch. This reduction arises from the PEV power restoration performed by the middle-level dispatch model. Fig. 12 shows the scheduled and dispatched PEV power of the proposed scheme. It can be observed that different degrees of PEV power restoration have occurred in most of the timeslots. Yet, compared with the best 3.54% CEL of the deterministic scheme, 10.9% loss is still relatively large. This relatively large CEL is a result of the proposed scheme using more PEV power to limit the net load variations to prevent the possible URC operations in consideration of WP uncertainty. The generous estimates of WP uncertainty intervals with *Q%* set to 96% also contribute to the relatively large CEL of the proposed scheme, since larger amount of PEV usage is needed to compensate for larger WP uncertainty.

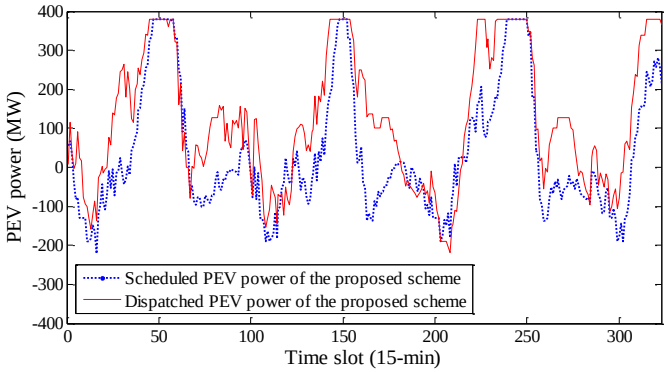

Fig. 12. Scheduled and dispatched PEV power profiles of the proposed scheme.

When the PEV charging needs to be further promoted, actions can be taken from the following four aspects. First, the construction of WP uncertainty intervals can be improved for more accurate modeling of WP uncertainty. For example,

This article has been accepted for publication in a future issue of this journal, but has not been fully edited. Content may change prior to final publication. Citation information: DOI 10.1109/TPWRS.2017.2696540, IEEE Transactions on Power Systems

instead of constructing a single set of WP uncertainty intervals, as the case in this paper, different sets of uncertainty intervals can be constructed for each hour of a day in a season. With more accurate WP uncertainty modeling, it can be expected that less amount of PEV usage will be needed to compensate for the WP uncertainty. Second, more constraints can be incorporated into the proposed scheme, such as the constraint on PEV charging completion. This, however, can compromise the effectiveness of the PEV-aided URC operation mitigation. Third, the URC operations of different units can be differentiated. Units designed to operate at varying load levels can have larger URC allowance. This leads to alleviated anti-URC regulation onus on PEVs, thus less impact will be imposed on the PEV charging, leading to smaller CEL. Lastly, enrolling more PEVs in the proposed scheme can also relieve the regulation onus on individual PEV for better fulfillment of the charging demand.

The statistics of PEV final SOC are summarized in Table IV. Here, PEVs are broadly categorized as adequately charged ($SOC \geq 80\%$) or undercharged ($SOC < 80\%$). Especially, a PEV with SOC ≥ 90% has satisfied its charging requirement. As shown in Table IV, 76.62% of the PEVs controlled by the proposed scheme have satisfied their charging requirements. This is prominently better than the 61.31% in the benchmark scheme. Additionally, 12.34% of the PEVs are undercharged in the benchmark scheme, whereas only 5.99% are undercharged in the proposed scheme. These results indicate that the heterogeneous charging requirements of individual PEVs can be better satisfied by using the decentralized charging control strategy of the proposed scheme.

TABLE IV
PEV FINAL SOC STATISTICS

Scheme	Proposed	Benchmark
Maximum SOC	91%	100%
Minimum SOC	62.64%	55.16%
PEVs with SOC in [90%, 100%] [a]	76.62%	61.31%
PEVs with SOC in [80%, 90%) [a]	17.39%	26.35%
PEVs with SOC in [70%, 80%) [a]	5.34%	9.46%
PEVs with SOC in [60%, 70%) [a]	0.65%	2.47%
PEVs with SOC in [50%, 60%) [a]	0%	0.41%

[a]expressed as percentages of the total number of PEVs

Overall, the proposed scheme achieves complete avoidance of URC operations while preserves most of the desired PEV charging energy. The benchmark scheme results in more URC operations and greater CEL than the proposed scheme and the deterministic scheme. Given that the benchmark scheme originates from typical BESS control methods, the simulation results indicate that it may not be good to directly apply the BESS control methods to the PEV power control for anti-URC regulation purposes, though the BESS control methods designed for limiting WP variations are straightforward and easy to implement. Thus, there is a need for a more effective charging control scheme specifically designed for PEVs to hedge against the URC operation, and this need has motivated the development of the proposed hierarchical scheme. Incurring only 3 URC operations with the minimum sacrifice of PEV charging energy, the deterministic scheme achieves the overall effectiveness comparable to that of the proposed scheme. Nevertheless, the proposed scheme is more robust to WP forecast errors than the deterministic scheme, which is shown in next section.

B. Simulation with Hypothetical Wind Power Profile

This section investigates the performances of the four schemes when subjected to severe WP fluctuations in unstable fast-moving weather. The hypothetical WP shown in Fig. 5(b) is adopted.

TABLE V
NO. OF URC OPERATIONS AND PEV CHARGING ENERGY LOSSES IN THE HYPOTHETICAL VERY FLUCTUATING WP SCENARIO

Scheme	1	2	3	4
Upward URC	73	14	22	15
Downward URC	70	7	16	16
Total URC	143	21	38	31
CEL in actual dispatch	0%	3.68%	20.41%	1.17%

Scheme 1–4 are the scheme with uncontrolled PEV charging, the proposed scheme, the benchmark scheme, and the deterministic scheme, respectively.

The number of URC operations and the associated CELs are summarized in Table V. As expected, quite a number of URC operations are incurred with uncontrolled PEV charging. The proposed scheme prominently outperforms the other schemes in mitigating the URC operations. CELs caused by the proposed scheme and the deterministic scheme are comparably small. Overall, the proposed scheme achieves better performance than the other schemes when facing severe WP fluctuations. This indicates that the proposed scheme is more capable of withstanding WP forecast errors.

VI. CONCLUSION

Increasing WP integration is notably changing the way conventional generators are operated. An important but somehow overlooked issue is the unit cycling, whose damaging effects are recognized but difficult to quantify as they may widely vary from one unit to another. Unlike most of the existing works whose primary concern is on the scarcity of generator ramping capability, this paper utilizes PEV power to hedge against the URC operations in a system with high WP penetration.

To the best of the authors' knowledge, this is a pioneering work to propose a general-form representation of the URC operation. The hierarchical structure of the proposed scheme consists of scheduling, dispatch, and control layers, which form a complete full-package solution for coordinating PEV power to hedge against the URC operation. The proposed scheme is compared with its deterministic version and the benchmark scheme. Simulation results show that with the WP uncertainty taken into account, the proposed scheme is more effective in mitigating URC operations while able to preserve most of the desired PEV charging energy. The proposed scheme is also shown to be more robust to severe WP fluctuations in unstable fast-moving weather condition, which indicates its greater capability to withstand WP forecast errors. With its guaranteed effectiveness in buffering conventional generators from the impact of WP variations, the proposed

scheme can be very helpful to future smart grids with high penetration of WP.

Three further works are planned. First, a comprehensive cost analysis is being conducted to examine the economic feasibility of the proposed scheme. Various price scenarios are considered to cover possible variations in the URC cost, the battery degradation cost, and the unfulfilled charging demand cost. Second, a more accurate PEV load model taking into account the uncertainties in PEV availability will be developed. These uncertainties would normally have adverse impact on the effectiveness of the PEV-aided URC operation mitigation. Thus, a method for properly addressing these uncertainties in the proposed scheme will be devised. Third, since the structure of the proposed scheme makes it suitable for being integrated into a multi-segment power market, a framework will be designed for the application of the proposed scheme in a market environment.

REFERENCES

[1] N. Kumar, P. Besuner, S. Lefton, D. Agan, and D. Hilleman, "Power Plant Cycling Costs," Intertek APTECH, Sunnyvale, CA, Tech. Rep. SR-5500-55433, Apr. 2012.

[2] N. Troy, E. Denny, and M. O'Malley, "Base-load cycling on a system with significant wind penetration," *IEEE Trans. Power Syst.*, vol. 25, no. 2, pp. 1088–1097, May 2010.

[3] N. Troy, D. Flynn, M. Milligan, and M. O'Malley, "Unit commitment with dynamic cycling costs," *IEEE Trans. Power Syst.*, vol. 27, no. 4, pp. 2196–2205, Nov. 2012.

[4] L. Deng, B. F. Hobbs and P. Renson, "What is the cost of negative bidding by wind? A unit commitment analysis of cost and emissions," *IEEE Trans. Power Syst.*, vol. 30, no. 4, pp. 1805–1814, Jul. 2015.

[5] P. Vithayasrichareon and I. F. MacGill, "Impacts of generation-cycling costs on future electricity generation portfolio investment," *2014 IEEE PES General Meeting*, National Harbor, MD, 2014, pp. 1–5.

[6] P. Rodilla, S. Cerisola and C. Batlle, "Modeling the major overhaul cost of gas-fired plants in the unit commitment problem," *IEEE Trans. Power Syst.*, vol. 29, no. 3, pp. 1001–1011, May 2014.

[7] C. Batlle and P. Rodilla, "An enhanced screening curves method for considering thermal cycling operation costs in generation expansion planning," *IEEE Trans. Power Syst.*, vol. 28, no. 4, pp. 3683–3691, Nov. 2013.

[8] E. Ela and M. O'Malley, "Studying the variability and uncertainty impacts of variable generation at multiple timescales," *IEEE Trans. Power Syst.*, vol. 27, no. 3, pp. 1324–1333, Aug. 2012.

[9] R. Huang, E. Farantatos, G. J. Cokkinides and A. P. Meliopoulos, "Impact of non-dispatchable renewables on generator cycling and control via a hierarchical control scheme," *Transmission and Distribution Conference and Exposition (T&D), 2012 IEEE PES*, Orlando, FL, 2012, pp. 1–8.

[10] K. W. Wee, S. S. Choi, and D. M. Vilathgamuwa, "Design of a least-cost battery–supercapacitor energy storage system for realizing dispatchable wind power," *IEEE Trans. Sustain. Energy*, vol. 4, no. 2, pp. 786–796, Apr. 2013.

[11] Q. Jiang and H. Wang, "Two-time-scale coordination control for a battery energy storage system to mitigate wind power fluctuations," *IEEE Trans. Energy Convers.*, vol. 28, no. 1, pp. 52–61, Mar. 2013.

[12] Q. Jiang, Y. Gong, and H. Wang, "A battery energy storage system dual-layer control strategy for mitigating wind farm fluctuations," *IEEE Trans. Power Syst.*, vol. 28, no. 3, pp. 3263–3273, Aug. 2013.

[13] X. Li, D. Hui, and X. Lai, "Battery energy storage station (BESS)-Based smoothing control of photovoltaic (PV) and wind power generation fluctuations," *IEEE Trans. Sustainable Energy*, vol. 4, no. 2, pp. 464–473, Apr. 2013.

[14] J. Tomic and W. Kempton, "Using fleets of electric-drive vehicles for grid support," *J. Power Sources*, vol. 168, no. 2, pp. 459–468, Jun. 2007.

[15] M. E. Khodayar, L. Wu, and M. Shahidehpour, "Hourly coordination of electric vehicle operation and volatile wind power generation in SCUC," *IEEE Trans. Smart Grid*, vol. 3, no. 3, pp. 1271-1279, Sep. 2012.

[16] H. Liu, Z. C. Hu, Y. H. Song, and J. Lin, "Decentralized vehicle-to-grid control for primary frequency regulation considering charging demands," *IEEE Trans. Power Syst.*, vol. 28, no. 3, pp. 3480-3489, Aug. 2013.

[17] Y. Ota, H. Taniguchi, T. Nakajima, K. M. Liyanage, J. Baba, and A. Yokoyama, "Autonomous distributed V2G (vehicle-to-grid) satisfying scheduled charging," *IEEE Trans. Smart Grid*, vol. 3, pp. 559-564, Mar. 2012.

[18] B. Zhang and M. Kezunovic, "Impact on power system flexibility by electric vehicle participation in ramp market," *IEEE Trans. Smart Grid*, vol. 7, no. 3, pp. 1285-1294, May 2016.

[19] C. T. Li, C. S. Ahn, H. Peng, and J. Sun, "Synergistic control of plug-in vehicle charging and wind power scheduling," *IEEE Trans. Power Syst.*, vol. 28, no. 2, pp. 1113-1121, May 2013.

[20] A. Bilh, K. Naik, and R. El-shatshat, "A novel online charging algorithm for electric vehicles under stochastic net-load," *IEEE Trans. Smart Grid* , to be published.

[21] Z. S. Zhang, Y. Z. Sun, D. W. Gao, J. Lin, and L. Cheng, "A versatile probability distribution model for wind power forecast errors and its application in economic dispatch," *IEEE Trans. Power Syst.* vol. 28, no. 3, pp. 3114–3125, Aug. 2013.

[22] W. F. Yao, J. H. Zhao, F. S. Wen, Y. S. Xue and G. Ledwich, "A hierarchical decomposition approach for coordinated dispatch of plug-in electric vehicles," *IEEE Trans. Power Syst.*, vol. 28, no. 3, pp. 2768–2778, Aug. 2013.

[23] Z. Xu, D. S. Callaway, Z. Hu and Y. Song, "Hierarchical coordination of heterogeneous flexible loads," *IEEE Trans. Power Syst.*, vol. 31, no. 6, pp. 4206-4216, Nov. 2016.

[24] H. Zhang, Z. Hu, Z. Xu and Y. Song, "Evaluation of achievable vehicle-to-grid capacity using aggregate PEV model," *IEEE Trans. Power Syst.*, vol. 32, no. 1, pp. 784-794, Jan. 2017.

[25] S. H. Madaeni and R. Sioshansi, "Measuring the benefits of delayed price-responsive demand in reducing wind-uncertainty costs," *IEEE Trans. Power Syst.*, vol. 28, no. 4, pp. 4118–4126, Nov. 2013.

[26] X. Luo, S. W. Xia, and K. W. Chan, "A simple decentralized charging control scheme of plug-in electric vehicles for alleviating wind farm intermittency," *Energy Procedia.*, vol. 61, pp. 1789–1792, Dec. 2014.

[27] C. Grigg, P. Wong, P. Albrecht, R. Allan, M. Bhavaraju, R. Billinton, Q. Chen, C. Fong, S. Haddad, S. Kuruganty, W. Li, R. Mukerji, D. Patton, N. Rau, D. Reppen, A. Schneider, M. Shahidehpour, and C. Singh, "The IEEE reliability test system—1996," *IEEE Trans. Power Syst.*, vol. 14, no. 3, pp. 1010–1018, Aug. 1999.

[28] Data sheet: 118bus abreu, Electrical and Computer Engineering Department of Illinois Institute of Technology, Online, http://motor.ece.iit.edu/Data (Accessed: 19 Nov. 2014).

[29] Wind power generation data, Elia, Online, http://www.elia.be/en/grid-data/power-generation/wind-power (Accessed: 23 Dec. 2014).

[30] Electricity data: price and demand, The Australian Energy Market Operator, Online, http://www.aemo.com.au/Electricity/Data/Price-and-Demand (Accessed: 12 Feb. 2015).

[31] A. Santos, N. McGuckin, H. Y. Nakamoto, D. Gay, and S. Liss, Summary of Travel Trends: 2009 National Household Travel Survey, U.S. Department of Transportation Federal Highway Administration, Washington, DC, USA, Rep. FHWA-PL-11022, Jun. 2011.

[32] Gurobi Optimizer Version 5.6.3, Gurobi Optimization, Inc., Houston, Texas, 2015.

Xiao Luo received the B.Eng. (Hons) and Ph.D. degrees in electrical engineering from The Hong Kong Polytechnic University, Hong Kong, China, in 2011 and 2016, respectively. He is currently an engineering trainee with Huadian Power International Corporation Limited, Beijing, China. His major research interests include demand side management, renewable energy sources, micro grid and power market.

Shiwei Xia (M'12) received the B.Eng. and M.Eng. degrees in electrical engineering from Harbin Institute of Technology, Harbin, China, in 2007 and 2009, respectively, and the Ph.D. degree in power systems from The Hong Kong Polytechnic University, Hung Hom, Hong Kong, in 2015. He then stayed with the department and worked as a Research Associate and subsequently as a Postdoctoral Fellow in 2015 and 2016. Currently, he is with the State Key Laboratory of Alternate Electrical Power System with Renewable Energy Sources, School of Electrical and Electronic Engineering, North China Electric Power University, Beijing, China. His research interests include security and risk analysis for power systems with renewable energies, distributed optimization and control of multiple sustainable energy sources in smart grid.

Ka Wing Chan (M'98) received the B.Sc. (Hons) and Ph.D. degrees in electronic and electrical engineering from the University of Bath, U.K., in 1988 and 1992, respectively. He currently is an Associate Professor and Associate Head in the Department of Electrical Engineering of the Hong Kong Polytechnic University. His general research interests include power system stability, analysis and control, power grid integration, security, resilience and optimization, demand response management, etc.

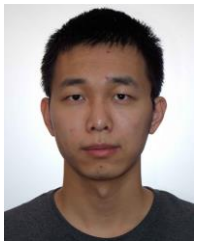

Xi LU received the B.Eng. degree in Electrical Engineering from North China Electric Power University in Beijing, China in 2015. He is currently pursuing the MPhil degree in Electrical Engineering at the Hong Kong Polytechnic University, Hong Kong. His research interests include application of robust optimization and distributionally robust optimization in power system operation.